Nanotechnology

PAPER

Thermal-controlled releasing and assembling of functional nanomembranes through polymer pyrolysis

To cite this article: Fei Ma *et al* 2019 *Nanotechnology* **30** 354001

IOP Publishing Nanotechnology

Nanotechnology **30** (2019) 354001 (10pp) https://doi.org/10.1088/1361-6528/ab1dcc

Thermal-controlled releasing and assembling of functional nanomembranes through polymer pyrolysis

Fei Ma[1], Borui Xu[1], Shuai Wu[2], Lu Wang[1], Biran Zhang[1], Gaoshan Huang[1], Ai Du[2], Bin Zhou[2] and YongFeng Mei[1]

[1] Department of Materials Science, Fudan University, Shanghai 200433, People's Republic of China
[2] Shanghai Key Laboratory of Special Artificial Microstructure Materials and Technology and School of Physics Science and Engineering, Tongji University, Shanghai 200092, People's Republic of China

E-mail: yfm@fudan.edu.cn

Received 28 January 2019, revised 17 April 2019
Accepted for publication 29 April 2019
Published 11 June 2019

Abstract

Pyrolysis, which involves thermal decomposition of materials at elevated temperatures, has been commonly applied in the chemical industry. Here we explored the pyrolysis process for 3D nanofabrication. By strain engineering of nanomembranes on a thermal responsive polymer as the sacrificial layer, we demonstrated that diverse 3D rolled-up microstructures with different functions could be achieved without any additional solution and drying process. We carefully studied the effect of molecular weight of the polymer in the pyrolysis process and identified that the rapid breakdown of molecular backbone to a monomer is the key for nanomembrane releasing and rolling. Preferential rolling direction and corresponding dynamics were studied by analyzing the real-time video of the rolling process. We further demonstrated the versatile functions of the fabricated 3D structures as catalytic microengines and optical resonators. The simple fabrication methodology developed here may have great potential in producing functional 3D tubular micro-/nanostructures.

Supplementary material for this article is available online

Keywords: polymer pyrolysis, 3D nanofabrication, rolled-up micro/nanostructure, microengine, optical resonator

(Some figures may appear in colour only in the online journal)

1. Introduction

Spontaneous curving and rolling behavior is very common in nature [1, 2], from plant growth and food production to polypeptide chains curling. Inspired by these phenomena, scientists in various fields have mimicked the natural assembling routes to fabricate complex 3D structures with intriguing composition and morphology at micro- and nanoscale. Recently, self-assembly becomes one of the most attractive manufacturing methods to fabricate 3D micro/nanostructures [3–5]. In particular, self-rolling as one of the self-assembly techniques has been widely applied in electronic engineering [6–13], photonics [14–16], micromechanic [17, 18], biohybrid nanomaterials [18–21], energy storage [22], nanomachine [23, 24], and lab in a tube system [25]. The technology was firstly reported more than a decade ago [26–29], where strained nanomembrane (e.g., InAs/GaAs) was grown on a sacrificial layer via molecular beam epitaxy. Strain-induced curling happened after the selective removal of the sacrificial layer, and thus rolled-up tubular structures were formed [30–32]. Different material systems were employed for the fabrication of micro/nanostructures based on this so-called rolled-up nanotechnology since then [33], and many applications have been demonstrated. For instance, a strained nanomembrane containing quantum dots was made to prepare ring resonators [34]. The release of the strained layer resulted in the red shift and enhanced emission signal of the resonator [35]. Magnetic driven artificial bacterial flagella were fabricated by the self-rolling of helical nanobelts and the obtained artificial flagella were suitable for swimming in liquid with low Reynolds number for potential biomedical applications *in vivo* or *in vitro* [36, 37]. Hybrid nanomembranes were also rolled into tubular structures for energy storage devices with improving reversibility and miniaturized dimensions [38, 39]. The main advantage of rolled-up nanotechnology is that various geometry encoding can be implanted in 2D nanomembrane in order to guide assembly of target 3D architecture [40, 41]. However, in conventional rolled-up process, the upper strained nanomembrane may also be affected during chemical etching of the sacrificial layer, and efforts have been dedicated to select suitable material combination for selective etching [42–44]. As an attempt to solve this problem, photoresist was engaged as the sacrificial layer and it can be removed by an organic etchant while the inorganic strained nanomembrane was kept almost intact [45]. However, it is still challenging because the etching involves a liquid environment, and the evaporation of liquid during the drying step causes the collapse of the micro/nanostructure due to the effect of surface tension [46, 47]. Therefore, supercritical drying might be used in previous investigations to avoid this problem [45]. It is worth noting that the liquid-based process also limits the selection of materials that can survive in the solution.

To overcome these shortcomings, in this work, we modified the rolled-up nanotechnology by using thermal degradable poly-α-methylstyrene (PAMS) as a sacrificial layer. The releasing and self-rolling were carried out at high temperature in N_2 atmosphere based on a thermally controlled polymer pyrolysis process. The wet etching and supercritical drying steps can thus be waived. The influence from the polymer molecular weight, the geometry of the rolled-up structures, the preferential rolling direction, as well as the corresponding rolling dynamics were studied in the present work. We further demonstrated that the obtained tubular structures can be used as a microengine and optical resonator for possible applications in the fields of drug delivery and biosensing.

2. Experimental section

2.1. Deposition of sacrificial layer and nanomembranes

PAMS with molecular weight (M_w) of 270 kDa, 470 kDa, 1200 kDa, and 1400 kDa were synthesized as described in previous references [48, 49], and obtained white powder was dispersed in toluene solvent. Then, PAMS solution (0.1 $g\,l^{-1}$) was spin-coated on silicon substrate to fabricate PAMS sacrificial layer (figure S1 is available online at stacks.iop.org/NANO/30/354001/mmedia). The thick of the PAMS layer is determined to be $\sim$200 nm (figure S2). In order to construct strained nanomembranes, active materials with various thicknesses and layered structures were deposited by e-beam evaporation under high vacuum ($<10^{-4}$ Pa). Shadow masks were used to pattern the deposited nanomembranes (figure S1).

2.2. Rolling process and characterizations

The samples were heated at 300 °C (Instec HCS600 heating stage) to release the nanomembrane (figure S1). At this temperature, PAMS sacrificial layer was degraded into monomer molecules [50]. Released prestrained nanomembranes were self-rolled into tubular microstructure, and this process was recorded by optical microscopy (Olympus BX51) with a CCD camera. Thermal analyses were conducted on SDT Q600 from TA Instruments. The powder samples were heated up to 800 °C at a linear heating rate of 10 $°C\,min^{-1}$ with nitrogen protection.

2.3. Fabrication of a self-propelled microengine

Microengines with tubular geometry were produced by rolling SiO/Cr/Pt (20/20/5 nm) multilayer nanomembranes. The prepared tubular microengines were placed in 0.50% H_2O_2 aqueous solution, and self-propelled locomotion was recorded by a high-speed camera (up to 200 frames/s) attached to an optical microscope.

2.4. Fabrication and characterization of optical resonator

In order to fabricate microtubular optical resonator, 10 nm SiO and 20 nm Y_2O_3 were deposited by e-beam evaporator sequentially. Pyrolysis process of the polymer results in the rolling of Y_2O_3/SiO nanomembrane (i.e., microtubular resonator). Optical property of the resonator was characterized by a Raman spectrometer (LabRAM HR Evolution, Horiba Jobin Yvon) at room temperature with a 532 nm laser.

3. Results and discussion

Figure 1(a) illustrates the schematic of the self-rolling process. The as-deposited sample consists of prestrained nanomembranes, PAMS layer (serving as sacrificial layer), and a silicon substrate from top to bottom. The nanomembrane was firstly deposited on the surface of the PAMS layer, and its geometry was defined via covering a shadow mask during e-beam evaporation. Upon heating to high temperature, long PAMS polymer chain was cleaved into gaseous monomer without residue [50, 51]. A possible chain-radical reaction during degradation of PAMS is presented in figure 1(b). The pyrolysis process by chain-radical reaction results in the formation of monomer α-methylstyrene, which leads to the release of the upper nanomembrane. The internal strain of nanomembrane causes the rolling behavior, resulting in the formation of rolled-up tubular microstructure (figure 1(a)).

Figure 1(c) presents a set of rolled-up microstructures obtained via the pyrolysis of the sacrificial layer. Here, microtubular structures consisting of Ge, Y_2O_3/ZrO_2, Ti/Cr/Pt, and Ti/Fe are demonstrated, proving the versatility in materials of the current approach. Furthermore, the geometry of the rolled-up structures can be altered with a shadow mask design. Figure 1(d) shows three different rolled-up structures generated from nanomembranes with different patterns. One can see that the rolled-up microtube with blunt ends was

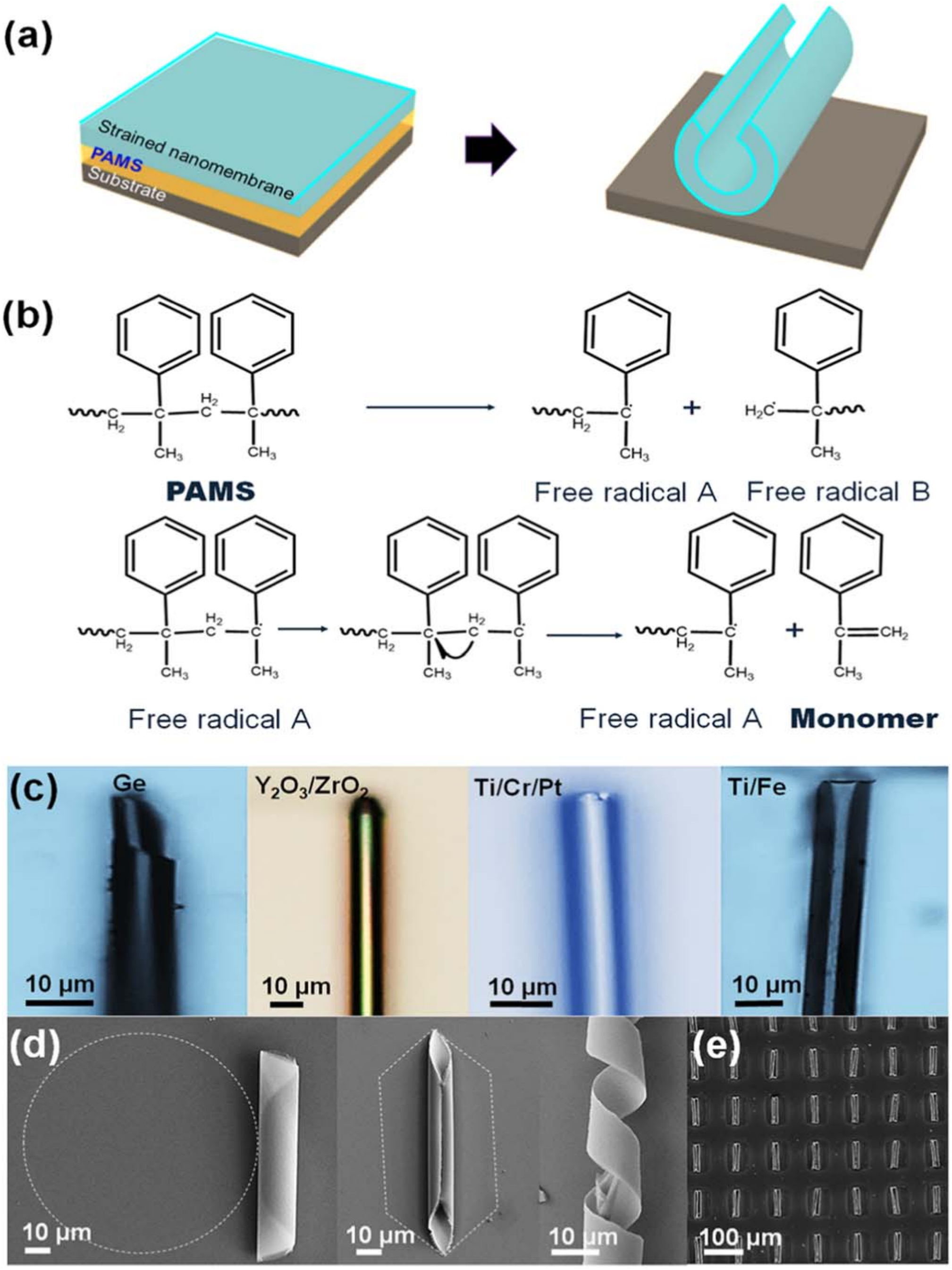

Figure 1. Rolled-up nanotechnology based on the pyrolysis process of PAMS. (a) Schematic illustration of the rolling of nanomembrane on a thermal degradable polymer. (b) Possible chain-radical reaction of PAMS. (c) Optical images of rolled-up microtubes made of Ge, Y_2O_3/ZrO_2, Ti/Cr/Pt, and Ti/Fe nanomembranes. (d) SEM images of rolled-up structures with different geometries: a microtube with blunt ends (left), a microtube with sharp ends (middle), and a microspring (right). Dashed lines in the left and middle panels indicate the shapes of original nanomembranes. (e) SEM image of an array of rolled-up SiO/Cr microtubes.

fabricated from circular nanomembrane (left panel of figure 1(d)). However, if the pattern was designed as an irregular diamond shape (middle panel of figure 1(d)), nanomembrane rolls from the long side, producing microtube with sharp ends. The right panel of figure 1(d) demonstrates that microspring can be fabricated if a misaligned angle exists between the rolling direction and the orientation of the stripe-shaped nanomembrane. We also demonstrate the ability of this approach in fabricated rolled-up structures in a highly ordered manner. In a typical image shown in figure 1(e), all the rolled-up microtubes in the array are well aligned along the same direction. In addition, although the current approach is not entirely compatible with conventional photolithography technology, our preliminary experimental results still demonstrated the possibility of patterning the nanomembrane on PAMS layer by a lithography step (see figure S3).

The molecular weight of the polymer should affect its pyrolysis temperature, as PAMS with high molecular weight

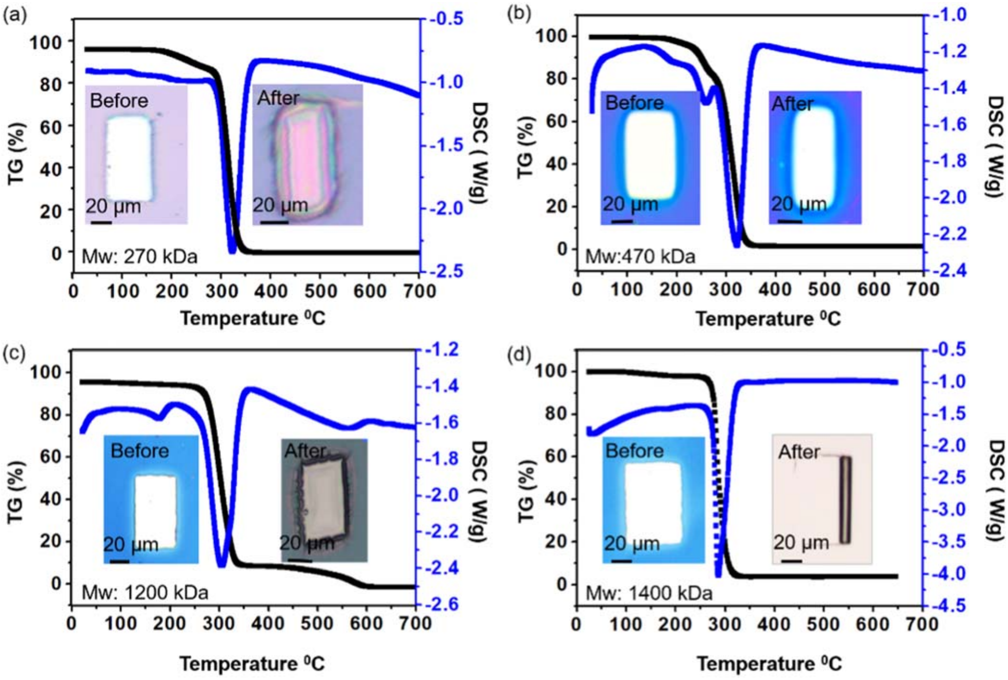

Figure 2. The TG and DSC curves of PAMS with Mw of (a) 270 kDa, (b) 470 kDa, (c) 1200 kDa, and (d) 1400 kDa. The insets show corresponding optical images of the SiO/Cr nanomembranes on PAMS layers before and after high temperature treatment at 300 °C for 5 min.

has low activation energy of decomposition [52]. Here, we also investigated the influence of molecular weight-related pyrolysis temperature on the self-rolling process. The thermogravimetry (TG) and differential scanning calorimetry (DSC) curves of PAMS with different molecular weights are shown in figure 2. TG curve presents change in mass with increasing temperature and DSC curve shows enthalpy change as a function of temperature. Endothermic peaks at 321, 320, 310, and 283 °C can be noticed on DSC curves of PAMS with M_w of 270 kDa, 470 kDa, 1200 kDa, and 1400 kDa, respectively, and obvious mass loss is observed in all TG curves. The heat absorption and mass loss demonstrated are mainly caused by radical reactions in figure 1(b). Besides, the pyrolysis of PAMS layers were further investigated by an optical method. In the experiment, PAMS layers were spin-coated on the quartz plates and placed on heating stage at 300 °C for 1 min. The experimental results in figure S4 in the supporting information show that the absorbance of PAMS with $M_w = 1400$ kDa is almost zero after heating, indicating that thermal degradation of PAMS with $M_w = 1400$ kDa occurs at 300 °C or below. We then checked the rolling behavior of nanomembranes on the PAMS layer. Rectangular patterned nanomembranes were deposited on the surfaces of PAMS layers with different M_w and the samples were then heated to 300 °C for 5 min. The experimental results are illustrated in the insets of figure 2, which also indicates that only PAMS with $M_w = 1400$ kDa can be degraded completely and microtubular structure is formed (insets in figure 2(d)). In contrast, PAMS with lower M_w (i.e., 270 kDa, 470 kDa, and 1200 kDa) cannot be sufficiently degraded, and no rolling process can be observed. However, the softening of PAMS layers and corresponding volume expansion lead to deformation and distortion of the upper nanomembranes (insets in figures 2(a)–(c)). As the temperature raised up to more than 300 °C, these PAMS layers could also get enough energy to pyrolysis into the gases monomer, and the above prestrained nanomembranes rolled up into different structures (figure S5). In the following discussion about rolled-up microtubular structures, only PAMS with $M_w = 1400$ kDa was used as the sacrificial layer.

In order to clarify the rolling process in detail, dynamic process of PAMS pyrolysis and rolling behavior during heating were also analyzed. Optical image of an array of SiO/Cr bilayer nanomembranes ($85 \times 45\ \mu m^2$) was captured and is shown in figure 3(a-I), and the changes in this array during heating process was studied. When the temperature is below the pyrolysis temperature of PAMS, no obvious change was noticed. When the temperature reaches pyrolysis temperature of PAMS, PAMS begins to degrade and cracks appear at the edge of the nanomembranes as depicted by the yellow arrows in figure 3(a-II). An interesting phenomenon is that the difference in degradation speed caused by temperature distribution leads to a crack generating at different times. After the crack forms, as degradation continues, the nanomembrane begin to roll and finally forms microtubes as shown in figure 3(a-III) (also see supporting movie S1). The time-dependent evolution of the above process is summarized in figure 3(b) for further investigation. Here, we focus on two parameters. The first one is the time when crack appears around the nanomembrane. The starting point t = 0 corresponds to the initiation of the first crack of the array, which locates around the lower-left nanomembrane (position: (1, 1)). The second parameter is the time difference between the crack initiation and the time when nanomembrane starts to roll. The

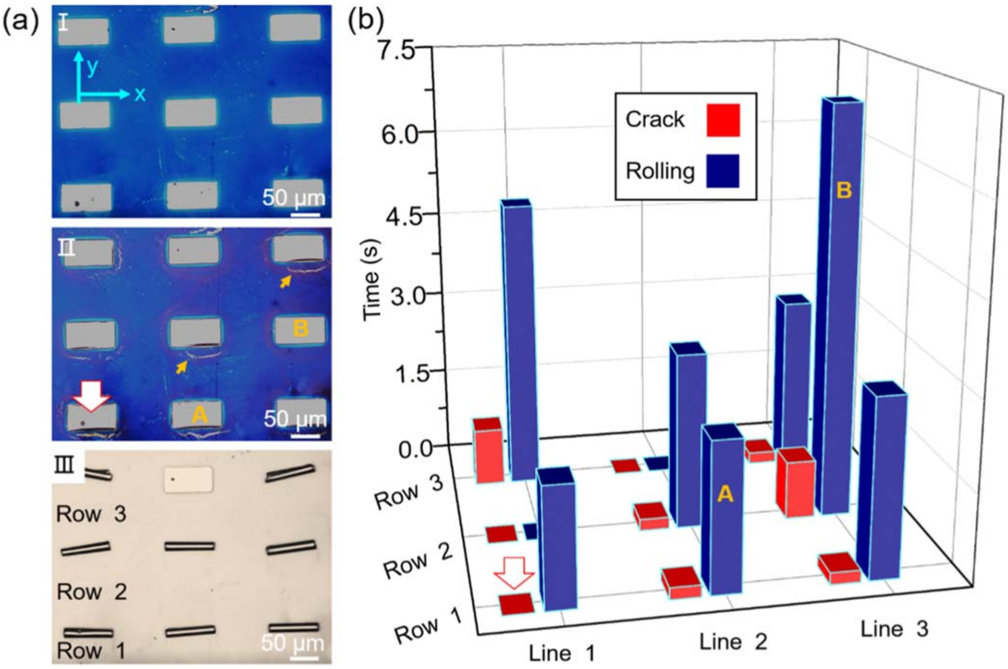

Figure 3. Time evolution of rolling process. (a) Optical microscopy image of the sample before and after the rolling process. The nanomembranes are SiO/Cr bilayer with the size of 85 × 45 μm^2. (b) The crack initiation (red bars) and the time difference between the crack initiation and the beginning of rolling (blue bars) for the nanomembrane array.

results in figure 3(b) reflect that an obvious difference in cracking and rolling processes for each nanomembrane exists. The cracks form fast in the lower-left region, and with increasing x and y, the formation of cracks is slower. For example, it is obvious that the crack initiation at position B (2, 3) lags behind that at position A (1, 2) for a few seconds. The shorter red bar for the generation of crack indicates higher temperature. The difference suggests the existence of temperature distribution on the surface of the sample. According to these results, a temperature gradient and corresponding thermal flow from lower-left corner to upper-right corner should exist in this sample. However, one can see that higher temperature does not guarantee that the nanomembrane starts to roll earlier (see blue bars in figure 3(b)). This phenonmenon will be discussed in the following paragraph.

Previous theoretical and experiment investigations show that preferential rolling direction depends on the aspect ratio of rectangular patterned nanomembrane [53]. However, in our present experiment, different rolling behaviors can be observed and are ascribed to the difference in crack generation, which determines the beginning of the rolling. In addition, the rolling direction does not depend on the aspect ratio only. We distinguish two general types of rolling behaviors: mixed side rolling (figure 4(a-I)) and mainly single long side rolling (figure 4(a-II)). When there are two or more cracks form around the nanomembrane (see Supporting Movies S2 and S4), the situation becomes complicated. Figure 4(a-I) shows the snapshots of rolling processes of nanomembranes with four cracks (panel 1) and two cracks (panel 2). In such cases, the nanomembranes are released from multiple directions simultaneously, and a competition between long side rolling and short side rolling can be observed. This may cause the rolling along diagonal direction, which is called as mixed rolling (figure 4(a-I)). We also found that the competition of the rolling along the two directions may take some time and thus the deterministic rolling behavior starts a little bit late, as shown in figure 3(b). On the other hand, as the crack forms only at long side, the nanomembrane is released therein and a rolling direction almost perpendicular to the long side is observed (figure 4(a-II)). The dynamics of this rolling process is further demonstrated in figure 4(b) as the captures from Supporting Movie S4. At 1 s after the beginning of rolling, the long side of the rectangular nanomembrane continues to roll. However, the release of the long side may not be simultaneous. The left part is still fixed, which leads to different rolling behaviors at different locations, as can be seen at 5.3 s in figure 4(b). At 6.3 s, the rolling process becomes the same for both the left and right parts. At 7 s, the left and right parts, again, demonstrate different rolling speeds, due to the influence from the fixed left short side. Finally, a complete rolled-up microtube is observed at 12 s.

As discussed above, the rolling direction is not just influenced by the aspect ratio of the patterned nanomembrane. The temperature gradient and corresponding thermal flow determine the crack formation and therefore affect the rolling direction significantly. This is meaningful if the rolled-up microspring is desired as the geometry of the microscpring can be controlled by altering the misaligned angle (α) between the rolling direction and the orientation of the stripe [54]. In present work, we fabricated microsprings with different geometries by changing α intentionally between 20° to 60°, and the results are demonstrated in figure 5(a). Since the geometrical parameters like diameter D, pitch p, and the helicity angle θ are related by $p = \pi D \tan \theta$ (see the diagram

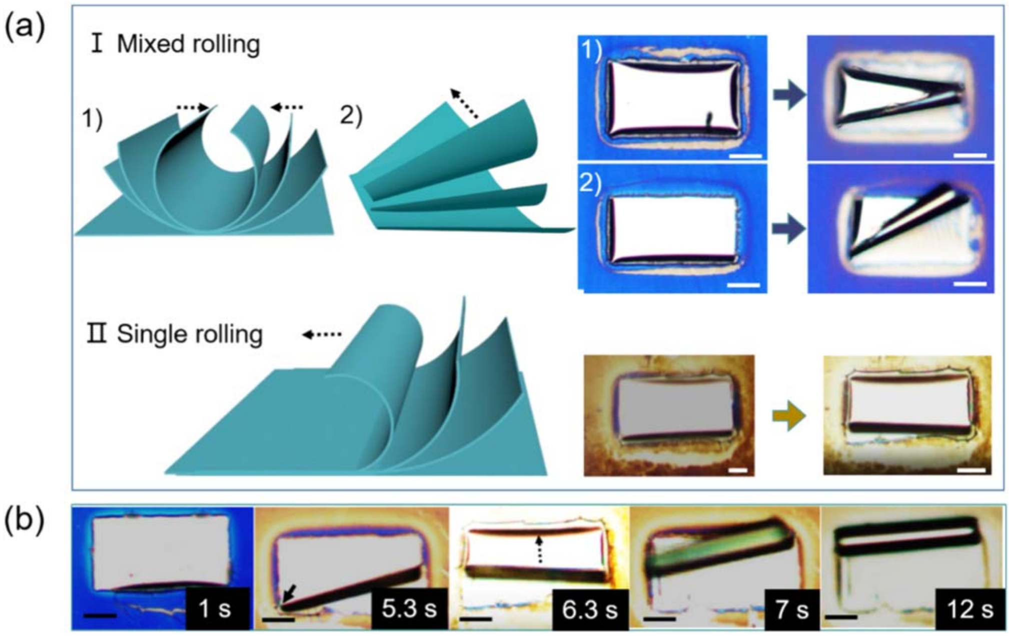

Figure 4. Rolling behavior of the rectangle-patterned SiO/Cr nanomembranes. (a) Schematic of two types of rolling behaviors: (I) mixed rolling and (II) single long side rolling. The corresponding optical images of the rolled-up structures are demonstrated. (b) Time evolution of long side rolling process. The scale bars is 20 μm.

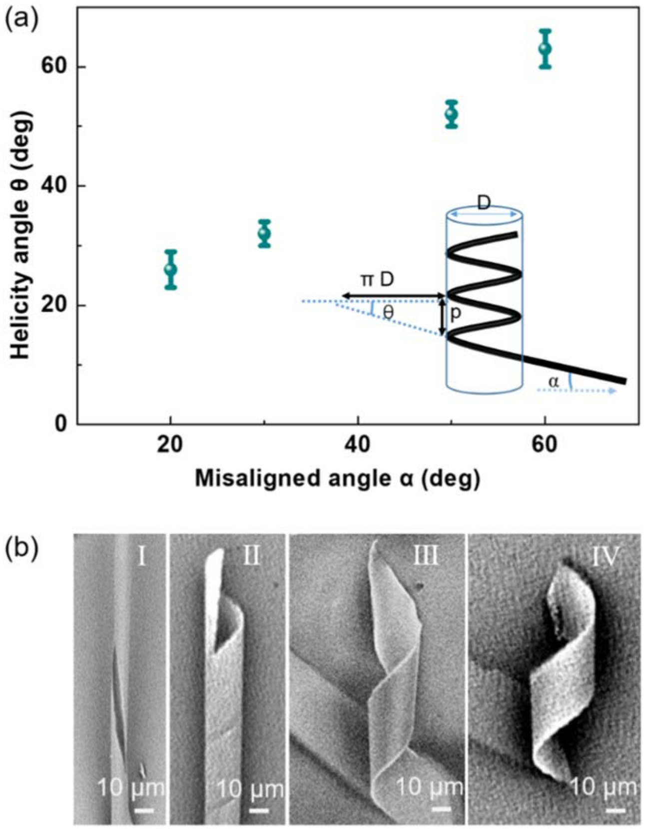

Figure 5. (a) Helicity angle of the microspring (θ) as the function of the misaligned angle (α) between the rolling direction and the orientation of the stripe-shaped nanomembrane. The inset illustrates the relation between pitch p, diameter D, misaligned angle α, and helicity angle θ. (b) SEM images of microsprings made from SiO/Cr bilayer stripes with different thicknesses: (I) 50/50 nm, (II) 58/58 nm, (III) 60/60 nm, and (IV) 63/63 nm.

in figure 5(a)), we therefore focus on the change of θ. The values of θ in figure 5(a) are obtained based on the statistics of several obtained microsprings. The calculated average θ values are 23°, 32°, 52°, and 63° corresponds to α of 20°, 30°, 50°, and 60°, respectively. One can see from figure 5(a) that θ always equals to α with small experimental uncertainty, which is consistent with the diagram in figure 5(a). Moreover, the diameter of the microspring is also an important geometrical parameter, and we noticed that the diameter could be tuned by changing the thickness of the nanomembrane. Figure 5(b) exhibits four typical microsprings fabricated by rolling SiO/Cr bilayer stripes. The diameters of (I) $\sim$ 8 μm, (II) $\sim$20 μm, (III) $\sim$25 μm, and (IV) $\sim$30 μm corresponds to stripe thicknesses of (I) 50/50 nm, (II) 58/58 nm, (III) 60/60 nm and (IV) 63/63 nm respectively. The results in figure 5 prove the deterministic rolling behavior and good controllability of the current approach.

Here, we hope to go deeper into the diameter control of the rolled-up structure. In general, self-rolling behavior is determined by strain gradient and elastic parameters of the nanomembrane [32, 33]. For instance, the expansion of the bottom layer upon release should cause a bilayer nanomembrane bending upwards, as schematically shown in the insets of figure 6. Practically, the diameter of the microtubular structure is determined by the strain status and the thickness of the nanomembrane [55, 56]. Previous investigation demonstrated that the diameter D can be theoretically predicted based on the Timoshenko formula [55, 56]:

$$\frac{1}{D} = \frac{3E'_1E'_2d_1d_2(d_1 + d_2)(\eta_1\varepsilon_1^0 - \eta_2\varepsilon_2^0)}{(E_1')^2d_1^4 + (E_2')^2d_2^4 + 2E_1'E_2'd_1d_2(2d_1^2 + 2d_2^2 + 3d_1d_2)} \tag{1}$$

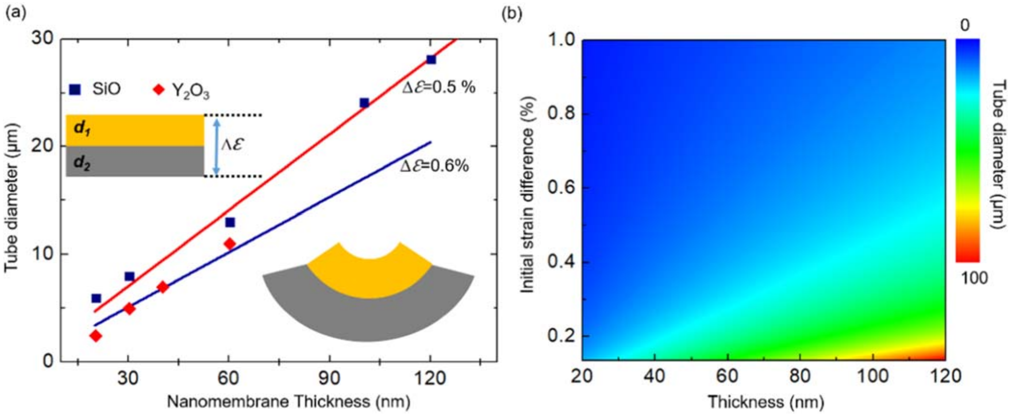

Figure 6. Diameter of the tubular structure as function of strain difference and nanomembrane thickness. (a) The blue and red cubes are experimental results, and the solid lines are calculated results with different strain gradients. The upper-left inset shows the initial strain status of upper (1) and lower (2) layers, which causes rolling of the nanomembrane (lower-right inset). The lower-right inset schematically shows a rolled-up bilayer nanomembrane. (b) Calculated diameter as the function of the SiO bilayer nanomembrane thickness and initial strain difference.

where d_i is the thickness, ε_i^0 is the initial strain in each layer, $E' = E/(1 - v^2)$, and $\eta = 1 + v$ (E and v are Young' s modulus and Poisson' s ratio, respectively). Subscripts $i = 1$ or 2 in the equation refer to the upper and lower layers, respectively. In our present work, as the two layers are made of same material, it is reasonable to set the elastic parameters of two layers as the same. So the diameter D of the rolled-up tubular structure is expressed as [57]:

$$D = \frac{(d_1 + d_2)^3}{3\Delta\varepsilon d_1 d_2} \tag{2}$$

where $\Delta\varepsilon = \varepsilon_1 - \varepsilon_2$. The change of the strain in the bilayer (i.e., ε_1 and ε_2) was introduced by change the deposition rate during e-beam evaporation [45]. In our work, rolled-up tubular structures made from SiO and Y_2O_3 nanomembranes were studies. For the sake of simplicity, the thicknesses of the upper and lower layers were chosen to be the same (i.e., $d_1 = d_2$) and the total thickness of the bilayer nanomembrane was used in the investigation. The diameters of the tubular structures were measured and are plotted in figure 6 as a function the total thickness of bilayer nanomembranes. Blue and red squares correspond to experimental results from SiO and Y_2O_3 nanomembranes respectively. With increasing thickness from 20 to 120 nm, the diameter of the microtube increases from 5 to ~30 μm. Here, we use the formula (2) to provide an estimation of the tube diameter. In this calculation, $\Delta\varepsilon$ are set as 0.5% and 0.6% as references, and obtained results are plotted as solid lines in figure 6(a). Small deviation may exist between experimental and theoretical results, but one can still see that SiO nanomembranes demonstrate a $\Delta\varepsilon$ of ~0.50% while Y_2O_3 nanomembranes normally possess a larger $\Delta\varepsilon$ of ~0.6%, possibly due to the difference during deposition process. Previous investigation demonstrated that the deposition rate, temperature, and chamber pressure had an influence on the strain status of deposited nanomembrane, which may be slightly different case by case [45]. We further plotted calculated tube diameter as a function of $\Delta\varepsilon$ and nanomembrane thickness in figure 6(b). It is clear that the tube diameter increases with the decrease of $\Delta\varepsilon$. Moreover, thicker nanomembrane with enhanced rigidity also causes a bigger diameter.

Finally, we present two examples to demonstrate the broad range of potential applications of current technology. Tubular catalytic microengines working with a bubble-propelling mechanism are one of the promising design [23], and rolled-up nanotechnology is commonly used to incorporate the catalyst layer into tube wall due to experimental convenience [58, 59]. In present work, we fabricated rolled-up SiO/Cr/Pt nanomembrane and engaged the obtained tubular structure as the catalytic microengine. The inner surface of the wall is Pt layer which can accelerate the decomposition of H_2O_2 into O_2. When O_2 microbubbles are expelled from the large end of the microtube, corresponding counter force pushes the microtube moving forward in opposite direction [60]. Figure 7(a) is obtained from real-time video of a typical SiO/Cr/Pt microengine moving in 0.5% H_2O_2 solution (supporting movie S5). However, one may note that the microengine does not move linearly. Due to the asymmetry of tubular structure, expelling of microbubbles deviates from the axis of the microtube and spin of the microengine is demonstrated. The results suggest that the motion behaviors can be easily tuned by the geometry of microtubes, which is realizable in rolled-up structures from nanomembranes with different pre-defined shapes. Investigation in this direction is currently in progress.

Moreover, rolled-up microtube can be used as an optical resonator due to the interference of the light circulating in the ring-like cross section. However, in a previous study, the rolled-up tubular micro-resonator was prepared by chemical etching in liquid, and part of the nanomembrane was connected with the substrate to fix the resonator [61]. This connection thus leads to obvious leakage of the light to the substrate [62]. Here, we should stress that our microtubular structures are produced based on the thermal degradation of PAMS and there is no connection between the microtube and the substrate. In such case, the light leakage to the substrate is significantly suppressed. Figure 7(b) shows the photoluminescence spectrum of a typical Y_2O_3/SiO (20/10 nm) microtubular resonator

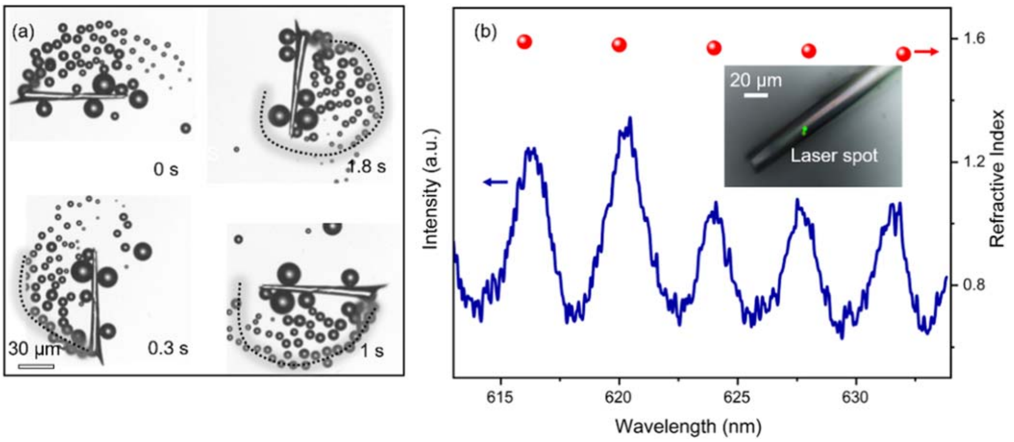

Figure 7. Applications of the rolled-up tubular structure fabricated with PAMS pyrolysis. (a) Selected video snapshots of a moving microengine with circular trajectory. (b) Photoluminescence spectrum of Y_2O_3/SiO microtube excited by 532 nm laser and the inset is optical image of the tested Y_2O_3/SiO mictotubular resonator. The position of the measured spot is marked. The red circles are effective refractive index obtained from the spectrum.

(the inset of figure 7(b)). Here, the effective refractive index n_{eff} of the tube wall can be calculated by using the following equation [61]:

$$n_{eff} = \frac{{\lambda_m}^2}{\Delta\lambda L} \tag{3}$$

where L is the circumference of the ring cross section (i.e., a circle) which equals to πD, λ_m is the resonance wavelength, $\Delta\lambda$ is space between the adjacent resonant peaks. The calculated n_{eff} is plotted in figure 7(b) as red circles. For Y_2O_3/SiO bilayer with thicknesses of 20 and 10 nm, respectively, the average refractive index $\bar{n}$ can be calculated by using the equation [34]:

$$\bar{n} = \frac{d_1 n_1 + d_2 n_2}{d_1 + d_2} \tag{4}$$

where n_1 and n_2 are refractive indexes of the two layers. The calculated average refractive index of the bilayer nanomembrane is ~1.67 in visible range, and is higher than the experimental effective refractive index. The reason is ascribed to the ultra-small thickness of tube wall. Here, the average tube wall thickness is 48 nm, which is much smaller than the light wavelength. Remarkable diffraction loss should exist due to the evanescent field [63].

4. Conclusions

In summary, in order to overcome the shortcoming of wet chemistry process in traditional rolled-up nanotechnology, we developed a feasible dry approach based on pyrolysis of a thermal degradable PAMS sacrificial layer. This sacrificial layer can be selectively removed at certain temperature in nitrogen, releasing the above nanomembrane, and 3D rolled-up structures with different geometries are thus assembled simultaneously. This approach avoids the complex corrosion procedure and supercritical drying step, providing great experimental convenience. We studied the diameter of the rolled-up structures with the help of the elastic mechanism. The release of the nanomembrane is also found to significantly influence the rolling behavior in terms of the rolling direction. We also explore the application potentials of the fabricated tubular structures in the fields of the microengine and optical micro-resonator. More applications from sophisticated 3D structures by rolling nanomembranes with predefined patterns in a 'dry' way can be expected in the future.

Acknowledgments

This work is supported by the National Natural Science Foundation of China (U1632115, 51711540298, 51475093 and 61628401), Science and Technology Commission of Shanghai Municipality (17JC1401700), the Changjiang Young Scholars Program of China and the Program of Shanghai Academic Research Leader (19XD1400600).

ORCID iDs

Gaoshan Huang https://orcid.org/0000-0002-0525-7177
YongFeng Mei https://orcid.org/0000-0002-3314-6108

References

[1] Xu S *et al* 2015 Assembly of micro/nanomaterials into complex, three-dimensional architectures by compressive buckling *Science* **347** 154–9

[2] Zhao Z L, Zhao H P, Chang Z and Feng X Q 2014 Analysis of bending and buckling of pre-twisted beams: a bioinspired study *Acta Mech. Sinica* **30** 507–15

[3] Rogers J A, Lagally M G and Nuzzo R G 2011 Synthesis, assembly and applications of semiconductor nanomembranes *Nature* **477** 45

[4] Whitesides G M and Boncheva M 2002 Beyond molecules: self-assembly of mesoscopic and macroscopic components *Proc. Natl Acad. Sci. USA* **99** 4769–74

[5] Jang K I *et al* 2017 A self-assembled three dimensional network designs for soft electronics *Nat. Commun.* **8** 15894

[6] Tian Z A, Xu B R, Hsu B, Stan L, Yang Z and Mei Y F 2018 Reconfigurable vanadium dioxide nanomembranes and microtubes with controllable phase transition temperatures *Nano Lett.* **18** 3017–23

[7] Guo Q L, Wang G, Chen D, Li G J, Huang G S, Zhang M, Wang X, Mei Y F and Di Z F 2017 Exceptional transport property in a rolled-up germanium tube *Appl. Phys. Lett.* **110** 112104

[8] Wang H, Zhen H L, Li S L, Jing Y L, Huang G S, Mei Y F and Lu W 2016 Self-rolling and light-trapping in flexible quantum well-embedded nanomembranes for wide-angle infrared photodetectors *Sci. Adv.* **2** e1600027

[9] Huang W *et al* 2018 Three-dimensional radio-frequency transformers based on a self-rolled-up membrane platform *Nat. Electron.* **1** 305–13

[10] Karnaushenko D, Kang T and Schmidt O G 2019 Shapeable material technologies for 3D self-assembly of mesoscale electronics *Adv. Mater. Technol.* **4** 1800692

[11] Torikai K, Oliveira R F, Camargo D H and Bufon C C 2018 Low-voltage, flexible, and self-encapsulated ultracompact organic thin-film transistors based on nanomembranes *Nano Lett.* **18** 5552–61

[12] Yoder M A, Yan Z, Han M D, Rogers J A and Nuzzo R G 2018 Semiconductor nanomembrane materials for high-performance soft electronic devices *J. Am. Chem. Soc.* **140** 9001–19

[13] Merces L, Oliveira R F and Bufon C C 2018 Nanoscale variable-area electronic devices: contact mechanics and hypersensitive pressure application *ACS Appl. Mater. Inter.* **10** 39168–76

[14] Tian Z A, Zhang L N, Fang Y F, Xu B R, Tang S W, Hu N, An Z H, Chen Z and Mei Y F 2017 Deterministic selfrolling of ultrathin nanocrystalline diamond -nanomembranes for 3D tubular/helical architecture *Adv. Mater.* **29** 1604572

[15] Lin X Y, Fang Y F, Zhu L G, Zhang J, Huang G S, Wang J and Mei Y F 2016 Self-rolling of oxide nanomembranes and resonance coupling in tubular optical microcavity *Adv. Opt. Mater.* **4** 936–42

[16] Strelow C, Rehberg H, Schultz C M, Welsch H, Heyn C, Heitmann D and Kipp T 2008 Optical microcavities formed by semiconductor microtubes using a bottlelike geometry *Phys. Rev. Lett.* **101** 127403

[17] Xu B R, Tian Z A, Wang J, Han H, Lee T and Mei Y F 2018 Stimuli-responsive and on-chip nanomembrane micro-rolls for enhanced macroscopic visual hydrogen detection *Sci. Adv.* **4** e8203

[18] Zhang Y H, Zhang F, Yan Z, Ma Q, Li X L, Huang Y G and Rogers J A 2017 Printing, folding and assembly methods for forming 3D mesostructures in advanced materials *Nat. Rev. Mater.* **2** 17019

[19] Gladman A S, Matsumoto E A, Nuzzo R G, Mahadevan L and Lewis J A 2016 Biomimetic 4D printing *Nat. Mater.* **15** 413

[20] Ko H J, Deravi L F, Park S J, Jang J G, Lee T H, Kang C, Lee J S, Parker K K and Shin K W 2017 Fabrication of millimeter-long carbon tubular nanostructures using the self-rolling process inherent in elastic protein layers *Adv. Mater.* **29** 1701732

[21] Cheng S Y, Jin Y, Wang N X, Cao F, Zhang W, Bai W, Zheng W F and Jiang X Y 2017 Self-adjusting, polymeric multilayered roll that can keep the shapes of the blood vessel scaffolds during biodegradation *Adv. Mater.* **29** 1700171

[22] Wang X F, Chen Y, Schmidt O G and Yan C L 2016 Engineered nanomembranes for smart energy storage devices *Chem. Soc. Rev.* **45** 1308–30

[23] Xu B R, Zhang B R, Wang L, Huang G S and Mei Y F 2018 Tubular micro/nanomachines: from the basics to recent advances *Adv. Funct. Mater.* **28** 1705872

[24] Hermanová S and Pumera M 2018 Polymer Platforms for Micro-and Nanomotor Fabrication *Nanoscale* **10** 7332–42

[25] Smith E J, Xi W, Makarov D, Mönch I, Harazim S, Quiñones V A B, Schmidt C K, Mei Y F, Sanchez S and Schmidt O G 2012 Lab-in-a-tube: ultracompact components for on-chip capture and detection of individual micro-/nanoorganisms *Lab Chip* **12** 1917–31

[26] Prinz V Y, Seleznev V A, Gutakovsky A K, Chehovskiy A V, Preobrazhenskii V V, Putyato M A and Gavrilova T A 2000 Free-standing and overgrown InGaAs/GaAs nanotubes, nanohelices and their arrays *Physica E* **6** 828–31

[27] Golod S V, Prinz V Y, Mashanov V I and Gutakovsky A K 2001 Fabrication of conducting GeSi/Si micro-and nanotubes and helical microcoils *Sci. Tech.* **16** 181

[28] Prinz V Y, Grützmacher D, Beyer A, David C, Ketterer B and Deckardt E 2001 A new technique for fabricating three-dimensional micro-and nanostructures of various shapes *Nanotechnology* **12** 399

[29] Schmidt O G and Eberl K 2001 Nanotechnology: thin solid films roll up into nanotubes *Nature* **410** 168

[30] Li Y *et al* 2017 Construction of small-diameter vascular graft by shape-memory and self-rolling bacterial cellulose membrane *Adv. Healthc. Mater.* **6** 1601343

[31] Huang M H, Boone C, Roberts M, Savage D E, Lagally M G, Shaji N, Qin H, Blick R, Nairn J A and Liu F 2005 Nanomechanical architecture of strained bilayer thin films: from design principles to experimental fabrication *Adv. Mater.* **17** 2860–4

[32] Chun I S, Challa A, Derickson B, Hsia K J and Li X L 2010 Geometry effect on the strain-induced self-rolling of semiconductor membranes *Nano Lett.* **10** 3927–32

[33] Li X L 2008 Strain induced semiconductor nanotubes: from formation process to device applications *J. Phys. D: Appl. Phys.* **41** 193001

[34] Kipp T, Welsch H, Strelow C, Heyn C and Heitmann D 2006 Optical modes in semiconductor microtube ring resonators *Phys. Rev. Lett.* **96** 077403

[35] Mendach S, Songmuang R, Kiravittaya S, Rastelli A, Benyoucef M and Schmidt O G 2006 Light emission and wave guiding of quantum dots in a tube *Appl. Phys. Lett.* **88** 111120

[36] Zhang L, Deckhardt E, Weber A, Schönenberger C and Grützmacher D 2005 Controllable fabrication of SiGe/Si and SiGe/Si/Cr helical nanobelts *Nanotechnology* **16** 655–63

[37] Zhang L, Abbott J J, Dong L, Peyer K E, Kratochvil B E, Zhang H, Bergeles C and Nelson B J 2009 Characterizing the swimming properties of artificial bacterial flagella *Nano Lett.* **9** 3663–7

[38] Bufon C C, Gonza J D, Thurmer D J, Grimm D, Bauer M and Schmidt O G 2010 Self-assembled ultra-compact energy storage elements based on hybrid nanomembranes *Nano Lett.* **10** 2506–10

[39] Huang S Z, Liu L X, Zheng Y, Wang Y, Kong D Z, Zhang Y M, Shi Y M, Zhang L, Schmidt O G and Yang H Y 2018 Efficient sodium storage in rolled-up amorphous Si nanomembranes *Adv. Mater.* **30** 1706637

[40] Bassik N, Stern G M and Gracias D H 2009 Microassembly based on hands free origami with bidirectional curvature *Appl. Phys. Lett.* **95** 091901

[41] Huang G S and Mei Y F 2012 Thinning and shaping solid films into functional and integrative nanomembranes *Adv. Mater.* **24** 2517–46

[42] Prinz V Y 2003 A new concept in fabricating building blocks for nanoelectronic and nanomechanic devices *Microelectron. Eng.* **69** 466–75

[43] Chun I S, Verma V B, Elarde V C, Kim S W, Zuo J M, Coleman J J and Li X 2008 InGaAs/GaAs 3D architecture formation by strain-induced self-rolling with lithographically defined rectangular stripe arrays *J. Cryst. Growth* **310** 2353–8

[44] Golod S V, Prinz V Y, Wägli P, Zhang L, Kirfel O, Deckhardt E, Glaus F, David C and Grützmacher D 2004 Freestanding SiGe/Si/Cr and SiGe/Si/SixNy/Cr microtubes *Appl. Phys. Lett.* **84** 3391–3

[45] Mei Y F, Huang G S, Solovev A A, Ureña E B, Mönch I, Ding F, Reindl T, Fu R K, Chu P K and Schmidt O G 2008 Versatile approach for integrative and functionalized tubes by strain engineering of nanomembranes on polymers *Adv. Mater.* **20** 4085–90

[46] Leong T G, Lester P A, Koh T L, Call E K and Gracias D H 2007 Surface tension-driven self-folding polyhedra *Langmuir* **23** 8747–51

[47] Nastaushev Y V, Prinz V Y and Svitasheva S N A 2005 Technique for fabricating Au/Ti micro-and nanotubes *Nanotechnology* **16** 908–12

[48] Shangguan X Y, Chen S F, Ma S, Liu M F, Tang C H, Yi Y and Zhang Z W 2018 Effect of molecular weight on the quality of poly (alpha-methylstyrene) mandrel *Matter and Radiation at Extremes* **2** 197–203

[49] Jones G D, Friedrich R E and Werkema T E 1956 Poly-alpha-methylstyrene *Ind. Eng. Chem.* **48** 2123–31

[50] Brown D W and Wall L A 1958 The pyrolysis of poly-α-methylstyrene *J. Phys. Chem.* **62** 848–52

[51] Yamamoto Y, Himei M and Hayashi K 1977 Radiation-induced pyrolysis of poly (α-methylstyrene). Degradation by cationic chain reactions *Macromolecules* **10** 1316–20

[52] Malhotra S L, Baillet C, Minh L and Blanchard L P 1978 Thermal decomposition of poly-α-methylstyrene *J. Macromol. Sci. Chem.* **12** 129–47

[53] Stoychev G, Zakharchenko S, Turcaud S, Dunlop J W and Ionov L 2012 Shape-programmed folding of stimuli-responsive polymer bilayers *ACS Nano* **6** 3925–34

[54] Li W M, Huang G S, Wang J, Yu Y, Wu X J, Cui X G and Mei Y F 2012 Superelastic metal microsprings as fluidic sensors and actuators *Lab Chip* **12** 2322–8

[55] Timoshenko S 1925 Analysis of Bi-metal thermostats *J. Opt. Soc. Am.* **11** 233–55

[56] Nikishkov G P 2003 Curvature estimation for multilayer hinged structures with initial strains *J. Appl. Phys.* **94** 5333–6

[57] Deneke C, Müller C, Phillipp N Y and Schmidt O G 2002 Diameter scalability of rolled-up In (Ga) As/GaAs nanotubes *Semicond. Sci. Technol.* **17** 1278–81

[58] Wang J and Gao W 2012 Nano/microscale motors: biomedical opportunities and challenges *ACS Nano* **6** 5745–51

[59] Li J X, Huang G S, Ye M M, Li M L, Liu R and Mei Y F 2011 Dynamics of catalytic tubular microjet engines: dependence on geometry and chemical environment *Nanoscale* **3** 5083–9

[60] Solovev A A, Mei Y F, Urena E B, Huang G S and Schmidt O G 2009 Catalytic microtubular jet engines self-propelled by accumulated gas bubbles *Small* **5** 1688–92

[61] Wang J, Song E M, Yang C L, Zheng L R and Mei Y F 2017 Fabrication and whispering gallery resonance of self-rolled up gallium nitride microcavities *Thin Solid Films* **627** 77–81

[62] Huang G S, Kiravittaya S, Bolaños Quiñones V A, Ding F, Benyoucef M, Rastelli A, Mei Y F and Schmidt O G 2009 Optical properties of rolled-up tubular microcavities from shaped nanomembranes *Appl. Phys. Lett.* **94** 141901

[63] Huang G S, Bolaños Quiñones V A, Ding F, Kiravittaya S, Mei Y F and Schmidt O G 2010 Rolled-up optical microcavities with subwavelength wall thicknesses for enhanced liquid sensing applications *ACS Nano* **4** 3123–30